JACS
JOURNAL OF THE AMERICAN CHEMICAL SOCIETY
Cite This: J. Am. Chem. Soc. 2019, 141, 8684−8688
Communication
pubs.acs.org/JACS

Oxidative Decarboxylase UndA Utilizes a Dinuclear Iron Cofactor

Olivia M. Manley,[†] Ruixi Fan,[‡] Yisong Guo,[‡] and Thomas M. Makris*[,†]

[†]Department of Chemistry and Biochemistry, University of South Carolina, Columbia, South Carolina 29208, United States
[‡]Department of Chemistry, Carnegie Mellon University, Pittsburgh, Pennsylvania 15213, United States

Supporting Information

ABSTRACT: UndA is a nonheme iron enzyme that activates oxygen to catalyze the decarboxylation of dodecanoic acid to undecene and carbon dioxide. We report the first optical and Mössbauer spectroscopic characterization of UndA, revealing that the enzyme harbors a coupled dinuclear iron cluster. Single turnover studies confirm that the reaction of the diferrous enzyme with dioxygen produces stoichiometric product per cluster. UndA is the first characterized example of a diiron decarboxylase, thus expanding the repertoire of reactions catalyzed by dinuclear iron enzymes.

Driven by potential application as biocatalysts for drop-in biofuel production, several enzymatic routes for hydrocarbon (alkane and 1-alkene) biosynthesis have been recently clarified.[1−6] A recurring theme in many of these enzymes is the involvement of a redox-active iron cofactor that is tuned for the C−C cleavage of a fatty acid or aldehyde, producing either a one-carbon CO_2[4,7] or formate[8] coproduct. These transformations represent novel reaction types for heme and nonheme iron enzymes.[9] In efforts to uncover the biochemical basis for 1-undecene production in many Pseudomonads, Zhang and colleagues adopted an elegant genomic screening strategy to identify the responsible gene (termed *undA*).[4] The *undA* stratagem for 1-olefin production is widely distributed in bacteria with over 1000 orthologs. This includes several important human pathogens where undecene is the major component of emitted volatile organic matter and can serve as an antifungal and antimicrobial agent.[10−12]

The *in vitro* reconstitution of UndA activity has shown that the decarboxylation of lauric acid to form undecene and a CO_2 coproduct strictly requires Fe^{2+} and dioxygen.[4] The medium chain-length (CL) specificity and cosubstrate requirement differ from the cytochrome P450 (CYP) fatty acid decarboxylase OleT. These variations offer discrete advantages for developing an *in vivo* platform for hydrocarbon production. For example, the preferred physiological substrate for OleT is a long CL (C_n = 20) fatty acid (FA),[2] and the metabolism of more biotechnologically attractive substrates (e.g., C_n = 12−16) often compromises chemoselectivity, producing unwanted hydroxy (typically at C_3) fatty acids that accompany the C_{n-1} olefin.[13,14] Despite numerous efforts to circumvent the H_2O_2 requirement by reconstituting OleT with biological redox chains and O_2,[15−17] the sluggish rates of electron transfer and inability of OleT to mediate proton delivery for O−O heterolysis appear to make the use of peroxide obligatory for efficient turnover.[18]

UndA was purported to utilize a mononuclear iron(II) cofactor based on metal-counting procedures and the presence of a single metal ion visible in the crystal structure of the reconstituted protein.[4] Based on analogy to OleT, FA decarboxylation would very likely involve hydrogen atom transfer (HAT) from the fatty acid β-carbon, a mechanism that is reiterated in the Fe(II)- and α-ketoglutarate (αKG)-dependent decarboxylases IsnB and AmbI3.[19,20] A unifying feature of OleT and the Fe(II)/αKG enzymes is the generation of a high-valent iron(IV)-oxo species for HAT, highlighting the necessity of forming a potent oxidant to carry out C−H abstraction at a largely unactivated carbon center.[7,19,21,22] The two reducing equivalents necessary for O−O heterolysis are provided by either H_2O_2 (OleT) or a combination of Fe(II) and the αKG cosubstrate (IsnB/AmbI3). On the basis of the mononuclear assignment and inability of UndA to produce undecene in the absence of exogenously added electrons, an iron(III)-superoxo species was posited as the C−H bond-cleaving intermediate. The equivalent species in CYPs is considered largely unreactive and is instead a branchpoint between the formation of Compound I and the unproductive release of superoxide.[23] However, some nonheme enzymes such as isopenicillin synthase (IPNS)[24] and the diiron myoinositol oxygenase (MIOX)[25] can utilize Fe-superoxide species to catalyze HAT on C−H bonds that are sufficiently activated by thiol or diol groups at adjacent carbon centers.

The Basic Local Alignment Search Tool (BLAST) revealed that UndA is similar (24% identity) to the chlamydial virulence factor CADD.[26] The precise biochemical role of CADD is not yet known, but it is strictly required in a pathway in *Chlamydia* for generating the *para*-aminobenzoic acid component of folate.[27] A carboxylate-bridged dinuclear metal center, presumed to be iron from metal analysis, is apparent in the CADD structure. Intriguingly, all of the metal-coordinating ligands of CADD are retained in UndA (Figures 1A and S1). We thus hypothesized that UndA may also accommodate two irons, which would provide the two electrons necessary to form a high-valent species. Indeed, such potent high-valent intermediates are well-known to be generated by dinuclear iron enzymes, best typified by soluble methane monooxygenase (sMMO), that performs one of the most difficult oxidation reactions in nature.[28]

We selected an ortholog from *P. syringae pv. tomato* DC3000 (*Ps*UndA) that is 79% identical to the structurally solved UndA from *P. aeruginosa* (*Pa*UndA) (Figure S1). All potential active-

Received: March 7, 2019
Published: May 14, 2019

DOI: 10.1021/jacs.9b02545
J. Am. Chem. Soc. 2019, 141, 8684−8688

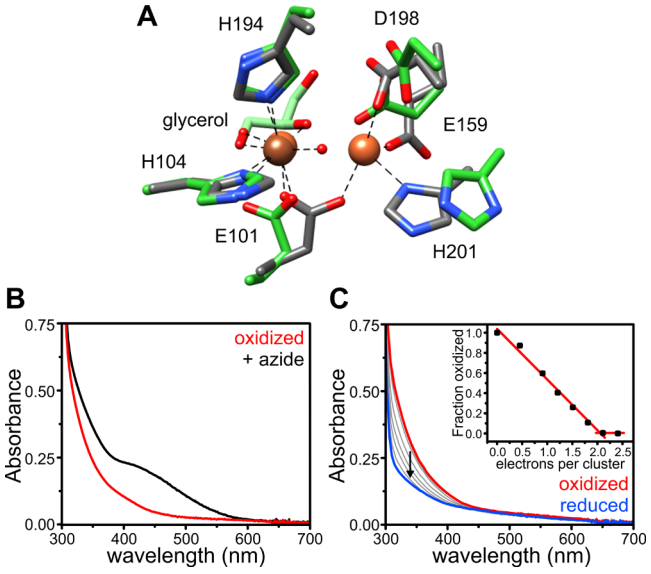

Figure 1. Structural alignment of *Pa*UndA (PDB: 4WWZ, green) with CADD (PDB: 1RCW, gray) (A). The iron atoms of CADD are shown in orange and that of mononuclear UndA is in brown. The optical spectrum of 75 μM UndA (iron-loaded) is shown as-isolated (red) and in the presence of 2 M sodium azide (black) (B). Titration of UndA with sodium dithionite results in conversion to the reduced state (blue) requiring ~2 reducing equivalents per cluster (C).

site metal-ligating residues that could form a diiron site in *Ps*UndA are conserved with both *Pa*UndA and CADD, and the protein was previously crystallized in an apo-form through structural genomics efforts (PDB: 3OQL) showing identical placement of putative metal−ligands. *Ps*UndA was heterologously expressed in *E. coli* and purified to homogeneity (Figure S2) by metal affinity chromatography as described in the Supporting Information (SI). When purified from bacterial cultures grown in LB medium with added $FeCl_3$, the iron content of *Ps*UndA is <0.2 mol equiv (Table S1), similar to the low metal yields reported for *Pa*UndA.[4] Fortuitously, the expression of *Ps*UndA in minimal medium and $FeCl_3$ enhanced the extent of iron-loading to as high as 1.1 mol equiv per protein. Inductively coupled plasma mass spectrometry revealed that the only other metal found in appreciable quantity was Ni, presumably an artifact from purification.

As-isolated, UndA exhibits a broad absorption band from 300 to 450 nm ($\varepsilon_{340} \approx 4$ mM^{-1} cm^{-1} assuming a cluster) (Figure 1B, red trace). The absorption is significantly more intense than that expected for nonheme, Fe^{2+}-dependent enzymes (e.g.,[29,30]). Titration of the enzyme with sodium dithionite results in bleaching of the chromophore and requires the addition of ~1 electron per iron (or two per cluster) to reach saturation, consistent with the presence of an Fe^{3+} center (Figure 1C). The dimetal assignment was substantiated through the addition of azide to the enzyme, a technique that has been used to successfully predict the cofactor in several carboxylate-bridged diiron enzymes.[31,32] Upon incubation with 2 M sodium azide, a protein-bound chromophore forms with absorption maxima at 350 and 440 nm (Figure 1B, black trace), owing to terminal ($\mu_{1,1}$) or bridging ($\mu_{1,3}$) ligation to one or both irons.[33]

Mössbauer spectroscopy of *Ps*UndA unambiguously demonstrates that a magnetically coupled dinuclear iron center is present and is the predominant form of the iron-loaded enzyme. The zero-field, 4.2-K spectrum of *Ps*UndA (Figures 2A and S3) is best simulated by two nested quadrupole

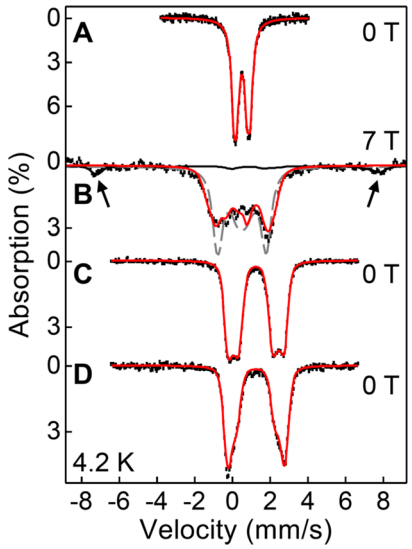

Figure 2. 4.2-K Mössbauer spectra of UndA in the as-isolated state measured under zero field (A) or 7 T applied field (B), the dithionite-reduced form (C), and the reduced state in the presence of C_{12} fatty acid (D) with experimental data shown in vertical black bar and the spectral simulation shown in red. The arrows in B indicate the outermost lines of a spectral feature that originates from a mononuclear ferric species; the corresponding simulation using a generic $S = 5/2$ ferric species is shown in the black solid line. The gray dashed line and the red line in B are the simulation assuming an $S = 0$ species and an exchange coupled species, respectively (see discussion in SI).

doublets with parameters indicative of high-spin ($S = 5/2$) ferric iron (Tables 1 and S3), consistent with those of other

Table 1. Parameters Used To Simulate the Mössbauer Spectra of UndA in the As-Isolated State, Reduced by Dithionite, and Reduced in the Presence of Dodecanoic Acid Substrate

UndA	δ (mm/s)	$\lvert\Delta E_Q\rvert$ (mm/s)	Line width (mm/s)[a]	Area (%)
As-isolated	0.51	0.88	0.32	43[b]
	0.50	0.53	0.34	43[b]
Dithionite-reduced	1.25	2.93	−0.5	48
	1.23	1.87	−0.55	52
Reduced + C_{12} FA	1.26	3.01	−0.5	65
	1.24	2.05	−0.5	35

[a]A negative line width in the simulation represents a Voigt line shape that is a convolution of a Gaussian and Lorentzian in 1:1 ratio. [b]A monoferric species accounts for the remaining absorption area.

enzymes containing magnetically coupled diferric centers (see SI for additional analysis).[31,32,34,35] The major feature obtained in a spectrum measured under an applied magnetic field of 7 T parallel to the γ radiation cannot be simulated as a strict diamagnetic species ($S = 0$) (Figure 2B, gray dashed line). A more reasonable simulation requires a small isotropic antiferromagnetic exchange interaction ($J \leq 15$ cm^{-1}) between the ferric centers with the inclusion of an antisymmetric exchange interaction (Figure 2B, red line, Figures S4−S6). A very similar situation was encountered in characterization of

DOI: 10.1021/jacs.9b02545
J. Am. Chem. Soc. 2019, 141, 8684−8688

the diferric state of sMMO.[36] The appearance of minor absorption peaks at ~ ± 8 mm/s in the high-field spectrum of oxidized UndA can be attributed to a small component (~15%) of the iron in the sample being in a magnetically isolated mononuclear ferric state,[37] likely arising from adventitiously bound iron or partially formed cluster.

Upon reduction with sodium dithionite, *Ps*UndA produces a Mössbauer spectrum (Figure 2C) that can also be simulated with two quadrupole doublets (Table 1, Figure S7). The larger isomer shifts of ~1.24 mm/s are consistent with high-spin ferrous iron. The requirement of two doublets to simulate both the diferric and diferrous states indicates that there are either two different types of clusters or that each iron in the cluster is distinguishable. Although neither of these possibilities can be rigorously ruled out, we currently favor the latter interpretation due to the equal areas and predicted asymmetry of the ligation. Nonetheless, the addition of excess dodecanoic acid to the diferrous state results in a significant perturbation of the spectrum (Figures 2D, S7–S8, Table 1). This structural alteration is very likely to arise from the direct ligation of FA, as suggested by cocrystal structures of mononuclear UndA with several FA substrate analogs.[4] The fact that most of the clusters are bound suggests a relatively high affinity of the enzyme for the C_{12} substrate, consistent with the single turnover studies that follow.

The catalytic activity of dinuclear *Ps*UndA was tested in single-turnover studies. The diferric enzyme was anaerobically reduced in the presence of 3 mol equiv of dodecanoic acid (relative to Fe-loaded protein) and subsequently exposed to excess O_2. Gas chromatography revealed the formation of undecene as the sole product of the reaction. The identity of the product was verified through comparison to an authentic standard by mass spectrometry (Figure S5). Product was not detected in reactions where the reductant, protein, or FA were omitted (Table S2). Based on the amount of cluster determined by Mössbauer, the amount of product formed is stoichiometric (0.92 ± 0.12) to cluster. Thus, the diferrous form is catalytically active and no accessory effector proteins nor additional reducing equivalents are required for turnover.

In summary, the spectroscopic and activity studies provide a firm basis for reassignment of UndA as a diiron enzyme. Oxidative decarboxylation represents a new chemical outcome for carboxylate-bridged diiron enzymes. By analogy to the aforementioned decarboxylases and established sMMO chemistry, a proposed mechanism for UndA is shown in Figure 3. The catalytic cycle proceeds from reaction of the diferrous FA-ligated ternary complex with O_2, consistent with the single turnover and Mössbauer studies presented here. The direct coordination of the FA to the cluster may be envisioned to serve a role in positioning the Cβ–H in such a way as to ensure HAT regiospecificity and for reinforcing C–C scission by thwarting oxygen rebound. It is enticing to invoke formation of a bis-Fe(IV) "Q" intermediate as the species responsible for Cβ HAT following O–O bond cleavage. Both closed-[38] and open-core[39] formulations are shown, either of which would be predicted to have ample oxidizing power to perform such a reaction. Further oxidation of the substrate through single electron transfer (SET) by an $Fe^{III}Fe^{IV}$ species would produce a carbocation or substrate-biradical that could rearrange to form CO_2 and undecene and restore the diferric resting state. Through analogy to the X intermediate of the R2 subunit of ribonucleotide reductase[40] and the consensus

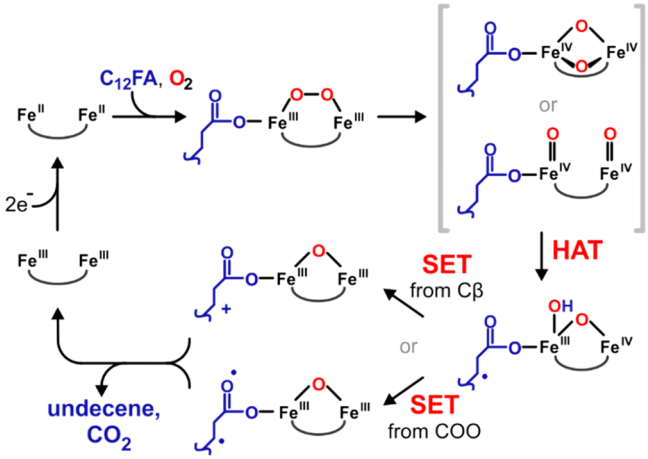

Figure 3. Proposed mechanism for the decarboxylation of fatty acids by UndA. The curved line represents bridging ligand(s). The remainder of the acyl chain of the fatty acid is abbreviated by a curved line.

dehydrogenation mechanism for desaturases,[41] an $Fe^{III}Fe^{IV}$ species should be able to satisfy such a role.

The 3-His/3 to 4 carboxylate ligand set used by UndA appears to be a flexible scaffold capable of diverse chemical transformations. In addition to FA decarboxylation by UndA and the cryptic oxidation that leads to pABA generation by CADD, a very similar coordination motif is employed by arylamine *N*-oxygenases[42,43] and likely common to enzymes that catalyze the halogenation of acyl carrier protein (ACP)-linked FAs,[44] *N*-nitrosation,[45] and the biosynthesis of alkene amino acids[46] (Figure S10). Thus, an intriguing question is what structural factors lead to differences in O_2-activation and elicit such dramatic reaction diversification.

■ ASSOCIATED CONTENT

Supporting Information

The Supporting Information is available free of charge on the ACS Publications website at DOI: 10.1021/jacs.9b02545.

Description of experimental procedures, Tables S1–S5, and Figures S1–S10 (PDF)

■ AUTHOR INFORMATION

Corresponding Author

*makrist@mailbox.sc.edu

ORCID

Yisong Guo: 0000-0002-4132-3565

Thomas M. Makris: 0000-0001-7927-620X

Notes

The authors declare no competing financial interest.

■ ACKNOWLEDGMENTS

This work was funded by the University of South Carolina Office of Research through the ASPIRE program and an NSF CAREER grant (CHE 155066) to T.M.M. Y.G. acknowledges the financial support from Carnegie Mellon University for this work.

■ REFERENCES

(1) Qiu, Y.; Tittiger, C.; Wicker-Thomas, C.; Le Goff, G.; Young, S.; Wajnberg, E.; Fricaux, T.; Taquet, N.; Blomquist, G. J.; Feyereisen, R. An insect-specific P450 oxidative decarbonylase for cuticular hydro-

DOI: 10.1021/jacs.9b02545
J. Am. Chem. Soc. 2019, 141, 8684–8688

carbon biosynthesis. *Proc. Natl. Acad. Sci. U. S. A.* **2012**, *109* (37), 14858−63.
(2) Rude, M. A.; Baron, T. S.; Brubaker, S.; Alibhai, M.; Del Cardayre, S. B.; Schirmer, A. Terminal olefin (1-alkene) biosynthesis by a novel p450 fatty acid decarboxylase from Jeotgalicoccus species. *Appl. Environ. Microbiol.* **2011**, *77* (5), 1718−27.
(3) Rui, Z.; Harris, N. C.; Zhu, X. J.; Huang, W.; Zhang, W. J. Discovery of a Family of Desaturase-Like Enzymes for 1-Alkene Biosynthesis. *ACS Catal.* **2015**, *5* (12), 7091−7094.
(4) Rui, Z.; Li, X.; Zhu, X.; Liu, J.; Domigan, B.; Barr, I.; Cate, J. H.; Zhang, W. Microbial biosynthesis of medium-chain 1-alkenes by a nonheme iron oxidase. *Proc. Natl. Acad. Sci. U. S. A.* **2014**, *111* (51), 18237−18242.
(5) Schirmer, A.; Rude, M. A.; Li, X.; Popova, E.; del Cardayre, S. B. Microbial biosynthesis of alkanes. *Science* **2010**, *329* (5991), 559−62.
(6) Sorigue, D.; Legeret, B.; Cuine, S.; Blangy, S.; Moulin, S.; Billon, E.; Richaud, P.; Brugiere, S.; Coute, Y.; Nurizzo, D.; Muller, P.; Brettel, K.; Pignol, D.; Arnoux, P.; Li-Beisson, Y.; Peltier, G.; Beisson, F. An algal photoenzyme converts fatty acids to hydrocarbons. *Science* **2017**, *357* (6354), 903−907.
(7) Grant, J. L.; Hsieh, C. H.; Makris, T. M. Decarboxylation of fatty acids to terminal alkenes by cytochrome P450 compound I. *J. Am. Chem. Soc.* **2015**, *137* (15), 4940−3.
(8) Warui, D. M.; Li, N.; Norgaard, H.; Krebs, C.; Bollinger, J. M.; Booker, S. J. Detection of Formate, Rather than Carbon Monoxide, As the Stoichiometric Coproduct in Conversion of Fatty Aldehydes to Alkanes by a Cyanobacterial Aldehyde Decarbonylase. *J. Am. Chem. Soc.* **2011**, *133* (10), 3316−3319.
(9) Wise, C. E.; Grant, J. L.; Amaya, J. A.; Ratigan, S. C.; Hsieh, C. H.; Manley, O. M.; Makris, T. M. Divergent mechanisms of iron-containing enzymes for hydrocarbon biosynthesis. *JBIC, J. Biol. Inorg. Chem.* **2017**, *22* (2−3), 221−235.
(10) Hunziker, L.; Bonisch, D.; Groenhagen, U.; Bailly, A.; Schulz, S.; Weisskopf, L. Pseudomonas strains naturally associated with potato plants produce volatiles with high potential for inhibition of Phytophthora infestans. *Appl. Environ. Microbiol.* **2015**, *81* (3), 821−30.
(11) Labows, J. N.; McGinley, K. J.; Webster, G. F.; Leyden, J. J. Headspace analysis of volatile metabolites of Pseudomonas aeruginosa and related species by gas chromatography-mass spectrometry. *J. Clin. Microbiol.* **1980**, *12* (4), 521−6.
(12) Lo Cantore, P.; Giorgio, A.; Iacobellis, N. S. Bioactivity of volatile organic compounds produced by Pseudomonas tolaasii. *Front. Microbiol.* **2015**, *6*, 1082.
(13) Hsieh, C. H.; Huang, X.; Amaya, J. A.; Rutland, C. D.; Keys, C. L.; Groves, J. T.; Austin, R. N.; Makris, T. M. The Enigmatic P450 Decarboxylase OleT Is Capable of, but Evolved To Frustrate, Oxygen Rebound Chemistry. *Biochemistry* **2017**, *56* (26), 3347−3357.
(14) Matthews, S.; Belcher, J. D.; Tee, K. L.; Girvan, H. M.; McLean, K. J.; Rigby, S. E.; Levy, C. W.; Leys, D.; Parker, D. A.; Blankley, R. T.; Munro, A. W. Catalytic Determinants of Alkene Production by the Cytochrome P450 Peroxygenase OleTJE. *J. Biol. Chem.* **2017**, *292* (12), 5128−5143.
(15) Dennig, A.; Kuhn, M.; Tassoti, S.; Thiessenhusen, A.; Gilch, S.; Bulter, T.; Haas, T.; Hall, M.; Faber, K. Oxidative Decarboxylation of Short-Chain Fatty Acids to 1-Alkenes. *Angew. Chem., Int. Ed.* **2015**, *54* (30), 8819−22.
(16) Fang, B.; Xu, H.; Liu, Y.; Qi, F.; Zhang, W.; Chen, H.; Wang, C.; Wang, Y.; Yang, W.; Li, S. Mutagenesis and redox partners analysis of the P450 fatty acid decarboxylase OleTJE. *Sci. Rep.* **2017**, *7*, 44258.
(17) Lu, C.; Shen, F. L.; Wang, S. B.; Wang, Y. Y.; Liu, J.; Bai, W. J.; Wang, X. Q. An Engineered Self-Sufficient Biocatalyst Enables Scalable Production of Linear alpha-Olefins from Carboxylic Acids. *ACS Catal.* **2018**, *8* (7), 5794−5798.
(18) Wise, C. E.; Hsieh, C. H.; Poplin, N. L.; Makris, T. M. Dioxygen Activation by the Biofuel-Generating Cytochrome P450 OleT. *ACS Catal.* **2018**, *8* (10), 9342−9352.
(19) Huang, J.-L.; Tang, Y.; Yu, C.-P.; Sanyal, D.; Jia, X.; Liu, X.; Guo, Y.; Chang, W.-c. Mechanistic Investigation of Oxidative Decarboxylation Catalyzed by Two Iron (II)-and 2-Oxoglutarate-Dependent Enzymes. *Biochemistry* **2018**, *57* (12), 1838−1841.
(20) Yu, C. P.; Tang, Y.; Cha, L.; Milikisiyants, S.; Smirnova, T. I.; Smirnov, A. I.; Guo, Y.; Chang, W. C. Elucidating the Reaction Pathway of Decarboxylation-Assisted Olefination Catalyzed by a Mononuclear Non-Heme Iron Enzyme. *J. Am. Chem. Soc.* **2018**, *140* (45), 15190−15193.
(21) Grant, J. L.; Mitchell, M. E.; Makris, T. M. Catalytic strategy for carbon-carbon bond scission by the cytochrome P450 OleT. *Proc. Natl. Acad. Sci. U. S. A.* **2016**, *113* (36), 10049−54.
(22) Yu, C.-P.; Tang, Y.; Cha, L.; Milikisiyants, S.; Smirnova, T. I.; Smirnov, A. I.; Guo, Y.; Chang, W.-c. Elucidating reaction pathway of decarboxylation-assisted olefination catalyzed by a mononuclear non-heme iron enzyme. *J. Am. Chem. Soc.* **2018**, *140*, 15190.
(23) Sligar, S. G.; Lipscomb, J. D.; Debrunner, P. G.; Gunsalus, I. C. Superoxide anion production by the autoxidation of cytochrome P450cam. *Biochem. Biophys. Res. Commun.* **1974**, *61* (1), 290−6.
(24) Tamanaha, E.; Zhang, B.; Guo, Y.; Chang, W. C.; Barr, E. W.; Xing, G.; St. Clair, J.; Ye, S.; Neese, F.; Bollinger, J. M., Jr.; Krebs, C. Spectroscopic Evidence for the Two C-H-Cleaving Intermediates of Aspergillus nidulans Isopenicillin N Synthase. *J. Am. Chem. Soc.* **2016**, *138* (28), 8862−74.
(25) Xing, G.; Diao, Y. H.; Hoffart, L. M.; Barr, E. W.; Prabhu, K. S.; Arner, R. J.; Reddy, C. C.; Krebs, C.; Bollinger, J. M. Evidence for C-H cleavage by an iron-superoxide complex in the glycol cleavage reaction catalyzed by myo-inositol oxygenase. *Proc. Natl. Acad. Sci. U. S. A.* **2006**, *103* (16), 6130−6135.
(26) Schwarzenbacher, R.; Stenner-Liewen, F.; Liewen, H.; Robinson, H.; Yuan, H.; Bossy-Wetzel, E.; Reed, J. C.; Liddington, R. C. Structure of the Chlamydia protein CADD reveals a redox enzyme that modulates host cell apoptosis. *J. Biol. Chem.* **2004**, *279* (28), 29320−29324.
(27) Adams, N. E.; Thiaville, J. J.; Proestos, J.; Juarez-Vazquez, A. L.; McCoy, A. J.; Barona-Gomez, F.; Iwata-Reuyl, D.; de Crecy-Lagard, V.; Maurelli, A. T. Promiscuous and Adaptable Enzymes Fill "Holes" in the Tetrahydrofolate Pathway in Chlamydia Species. *mBio* **2014**, *5* (4), DOI: 10.1128/mBio.01378-14.
(28) Lee, S. K.; Fox, B. G.; Froland, W. A.; Lipscomb, J. D.; Munck, E. A Transient Intermediate of the Methane Monooxygenase Catalytic Cycle Containing an Fe(Iv)Fe(Iv) Cluster. *J. Am. Chem. Soc.* **1993**, *115* (14), 6450−6451.
(29) Miller, M. A.; Lipscomb, J. D. Homoprotocatechuate 2,3-dioxygenase from Brevibacterium fuscum. A dioxygenase with catalase activity. *J. Biol. Chem.* **1996**, *271* (10), 5524−35.
(30) Price, J. C.; Barr, E. W.; Tirupati, B.; Bollinger, J. M., Jr.; Krebs, C. The first direct characterization of a high-valent iron intermediate in the reaction of an alpha-ketoglutarate-dependent dioxygenase: a high-spin FeIV complex in taurine/alpha-ketoglutarate dioxygenase (TauD) from Escherichia coli. *Biochemistry* **2003**, *42* (24), 7497−508.
(31) Fox, B. G.; Shanklin, J.; Somerville, C.; Münck, E. Stearoyl-acyl carrier protein delta 9 desaturase from Ricinus communis is a diiron-oxo protein. *Proc. Natl. Acad. Sci. U. S. A.* **1993**, *90* (6), 2486−2490.
(32) Makris, T. M.; Chakrabarti, M.; Münck, E.; Lipscomb, J. D. A family of diiron monooxygenases catalyzing amino acid beta-hydroxylation in antibiotic biosynthesis. *Proc. Natl. Acad. Sci. U. S. A.* **2010**, *107* (35), 15391−15396.
(33) Ai, J. Y.; Broadwater, J. A.; Loehr, T. M.; SandersLoehr, J.; Fox, B. G. Azide adducts of stearoyl-ACP desaturase: A model for mu-1,2 bridging by dioxygen in the binuclear iron active site. *JBIC, J. Biol. Inorg. Chem.* **1997**, *2* (1), 37−45.
(34) Fox, B. G.; Hendrich, M. P.; Surerus, K. K.; Andersson, K. K.; Froland, W. A.; Lipscomb, J. D.; Munck, E. Mossbauer, Epr, and Endor Studies of the Hydroxylase and Reductase Components of Methane Monooxygenase from Methylosinus-Trichosporium Ob3b. *J. Am. Chem. Soc.* **1993**, *115* (9), 3688−3701.
(35) Xing, G.; Hoffart, L. M.; Diao, Y. H.; Prabhu, K. S.; Arner, R. J.; Reddy, C. C.; Krebs, C.; Bollinger, J. M. A coupled dinuclear iron cluster that is perturbed by substrate binding in myo-inositol oxygenase. *Biochemistry* **2006**, *45* (17), 5393−5401.

DOI: 10.1021/jacs.9b02545
J. Am. Chem. Soc. 2019, 141, 8684−8688

(36) Kauffmann, K. E.; Popescu, C. V.; Dong, Y. H.; Lipscomb, J. D.; Que, L.; Munck, E. Mossbauer evidence for antisymmetric exchange in a diferric synthetic complex and diferric methane monooxygenase. *J. Am. Chem. Soc.* **1998**, *120* (34), 8739−8746.
(37) Que, L. *Physical methods in bioinorganic chemistry: spectroscopy and magnetism*; University Science Books: Sausalito, CA, 2000; p. vii, 556 pp.
(38) Shu, L. J.; Nesheim, J. C.; Kauffmann, K.; Munck, E.; Lipscomb, J. D.; Que, L. An (Fe_2O_2)-O-IV diamond core structure for the key intermediate Q of methane monooxygenase. *Science* **1997**, *275* (5299), 515−518.
(39) Cutsail, G. E., 3rd; Banerjee, R.; Zhou, A.; Que, L., Jr.; Lipscomb, J. D.; DeBeer, S. High-Resolution Extended X-ray Absorption Fine Structure Analysis Provides Evidence for a Longer Fe···Fe Distance in the Q Intermediate of Methane Monooxygenase. *J. Am. Chem. Soc.* **2018**, *140* (48), 16807−16820.
(40) Bollinger, J. M., Jr.; Edmondson, D. E.; Huynh, B. H.; Filley, J.; Norton, J. R.; Stubbe, J. Mechanism of assembly of the tyrosyl radical-dinuclear iron cluster cofactor of ribonucleotide reductase. *Science* **1991**, *253* (5017), 292−8.
(41) Shanklin, J.; Guy, J. E.; Mishra, G.; Lindqvist, Y. Desaturases: emerging models for understanding functional diversification of diiron-containing enzymes. *J. Biol. Chem.* **2009**, *284* (28), 18559−63.
(42) Choi, Y. S.; Zhang, H.; Brunzelle, J. S.; Nair, S. K.; Zhao, H. In vitro reconstitution and crystal structure of p-aminobenzoate N-oxygenase (AurF) involved in aureothin biosynthesis. *Proc. Natl. Acad. Sci. U. S. A.* **2008**, *105* (19), 6858−63.
(43) Knoot, C. J.; Kovaleva, E. G.; Lipscomb, J. D. Crystal structure of CmlI, the arylamine oxygenase from the chloramphenicol biosynthetic pathway. *JBIC, J. Biol. Inorg. Chem.* **2016**, *21* (5−6), 589−603.
(44) Nakamura, H.; Schultz, E. E.; Balskus, E. P. A new strategy for aromatic ring alkylation in cylindrocyclophane biosynthesis. *Nat. Chem. Biol.* **2017**, *13* (8), 916−921.
(45) Ng, T. L.; Rohac, R.; Mitchell, A. J.; Boal, A. K.; Balskus, E. P. An N-nitrosating metalloenzyme constructs the pharmacophore of streptozotocin. *Nature* **2019**, *566* (7742), 94−99.
(46) Marchand, J. A.; Neugebauer, M. E.; Ing, M. C.; Lin, C. I.; Pelton, J. G.; Chang, M. C. Y. Discovery of a pathway for terminal-alkyne amino acid biosynthesis. *Nature* **2019**, *567* (7748), 420−424.

DOI: 10.1021/jacs.9b02545
J. Am. Chem. Soc. 2019, 141, 8684−8688